KINEMATICS OF 2-D TRANSIENT WATER WAVES USING LASER DOPPLER ANEMOMETRY

By Cheung H. Kim,[1] Robert E. Randall,[2] Members, ASCE, Sung Y. Boo,[3] and Martin J. Krafft[4]

ABSTRACT: Results of recent research on experimental investigation of wave-fluid particle kinematics just prior to breaking using laser Doppler anemometry are presented. Extreme transient waves, similar to those found in hurricane Camille, and an "equivalent" regular wave, often used for design purposes, are generated and their kinematics measured. The kinematics of transient waves of smaller height are also measured to evaluate the effect of wave height, and these data are compared to Stokes third-order theory. Due to particular asymmetries not present in the large regular symmetric wave, the transient wave kinematics under the crest are shown to be much more severe above the still water level and somewhat less severe below. The stretching method used for the simulated transient wave underestimates the horizontal velocities in the crest and overestimates them below the still water level. These comparisons suggest that it would be worthwhile to further investigate the use of extreme waves as more realistic design waves and to develop a wave theory that accounts for the effect of the asymmetries.

INTRODUCTION

Fixed offshore structures typically consist of many slender cylinders as support legs and cross members and are fixed to the seafloor with piles driven through the legs and deep into the ocean floor. Compliant offshore structures usually have large cylinders in the floating structure and are moored to the sea floor by tendons or cables that are considered slender cylinders. The ocean environment consisting of winds, currents, and waves interacts with these structures to produce complex fluid loadings that are difficult to evaluate. However, practical techniques have been established for establishing wave loads under limited conditions, such as the Morison equation for slender bodies and diffraction theory for large structures. Morison's equation requires the determination of inertia and drag coefficients and knowledge of the fluid kinematics resulting from wave and current interaction under the wave surface, in the absence of any structure.

It is customary in the determination of wave kinematics to employ either a random wave or deterministic design wave approach. The random wave (time series) is obtained from the energy spectra for the design sea state, whereas the design wave (characterized only by height and period) is derived statistically as the most probable, largest wave at the design location for a given return period. Random wave approaches (Forristall 1981; Vugts and Bosma 1981; Rodenbusch and Forristall 1986) use linear wave theory and

[1]Assoc. Prof., Oc. Engrg. Program, Civ. Engrg. Dept., Texas A&M Univ., College Station, TX 77843.
[2]Assoc. Prof., Oc. Engrg. Program, Civ. Engrg. Dept., Texas A&M Univ., College Station, TX.
[3]Grad. Res. Asst., Oc. Engrg. Program, Civ. Engrg. Dept., Texas A&M Univ., College Station, TX.
[4]Oc. Engr., SOFEC, Houston, TX 77079.

Note. Discussion open until August 1, 1992. To extend the closing date one month, a written request must be filed with the ASCE Manager of Journals. The manuscript for this paper was submitted for review and possible publication on September 25, 1990. This paper is part of the ***Journal of Waterway, Port, Coastal, and Ocean Engineering***, Vol. 118, No. 2, March/April, 1992. ©ASCE, ISSN 0733-950X/92/0002-0147/$1.00 + $.15 per page. Paper No. 544.

the linear random superposition principle in conjunction with the "Wheeler or delta stretching" techniques (Wheeler 1970; Forristall 1981) to evaluate water particle kinematics. Gudmestad (1990) developed a new approach for estimating the kinematics under irregular waves, which was based on previous studies (Gudmestad and Connor 1986). The design wave kinematics can be determined from a variety of wave theories (Dean and Dalrymple 1984) including Airy, Stokes second through fifth order, cnoidal, and stream function, which are then used to estimate the design wave loads.

Recent progress in gathering and analyzing storm sea surface data, for instance (Ward 1974; Buckley 1983; Buckley and Stavovy 1981), has been a significant contribution to the research community studying extreme waves and wave loadings on marine structures. For example, an analysis of data from the Gulf of Mexico hurricane "Camille" and a storm off the Irish Coast (Buckley 1983) revealed that some of the largest waves contained in sample time histories were steep on their foreward face and greatly elevated. Such waves are often termed *extreme transient waves*.

Extreme transient waves have been modeled in a few wave tanks and reported by researchers such as Mansard and Funke (1982), Kjeldsen et al. (1980), Longuet-Higgins (1974), Rapp (1986), Takezawa and Hirayama (1977), Krafft and Kim (1987), and Kim et al. (1990). Kinematic measurements of extreme waves made by Kjeldsen et al. 1980) and Kjeldsen (1984) with electromagnetic current meters indicate crest velocities 36% greater than the phase velocity just prior to breaking, and prompted them to propose that combinations of severely asymmetric transient waves be selected as design waves, in order to avoid severe underestimation of wave loads.

Studies of the kinematics of breaking waves by Dommermuth et al. (1988) employed a potential theory for predicting wave elevation and velocity and used laser Doppler anemometry (LDA) to measure fluid velocities under the wave surface including the region above the still water level (SWL). Numerical results from the potential theory compared well with the laboratory experiments. Birkinshaw et al. (1988) investigated the kinematics of spilling breakers for the design of a small offshore gas platform. Using LDA to measure velocities in the wave crest, they found that values predicted from stream function wave theory were exceeded by 20%. Skjelbreia (1987) made extensive LDA measurements of fluid velocities under solitary waves breaking on a sloped bottom and computed the corresponding accelerations.

Kim et al. (1990) reported LDA measurements of velocity under the crest of a laboratory-generated 25-cm extreme transient wave that had a similar elevation profile as that found in hurricane Camille data (Buckley 1983). The maximum measured velocity just prior to breaking was found to be 1.47 m/s, which was 64% of the measured phase velocity of the transient wave and 184% of the velocity measured at the same elevation under a similar height Stokes wave. These measurements demonstrated the unique capability of the LDA to measure kinematics in the crest region of waves. The results also indicated the need to include the effects of extreme wave asymmetries in estimating maximum loads on offshore structures.

The objectives of this paper are to discuss the kinematics measured under laboratory-generated transient waves of different wave height using a laser Doppler anemometer, to describe the acceleration values that were determined numerically from the measured velocity data, to examine the wave height effect on the crest velocities, to compare the kinematics in the wave crest to those predicted by stretching the simulated transient wave and Stokes third-order theory, and to demonstrate differences in the kinematics

of an extreme transient wave and a regular wave of the type often considered as a "design" wave in preliminary investigations of maximum loads.

Accordingly, experimental measurements of particle velocities were conducted under the crest of various height asymmetric transient waves, and the results are compared with those from Stokes third-order theory and Wheeler's stretching technique. A large regular wave, approximating a Stokes third-order wave, with similar height and period as the transient wave was also created in the laboratory, and kinematic measurements were made and compared with those obtained for the transient wave. Due to particular

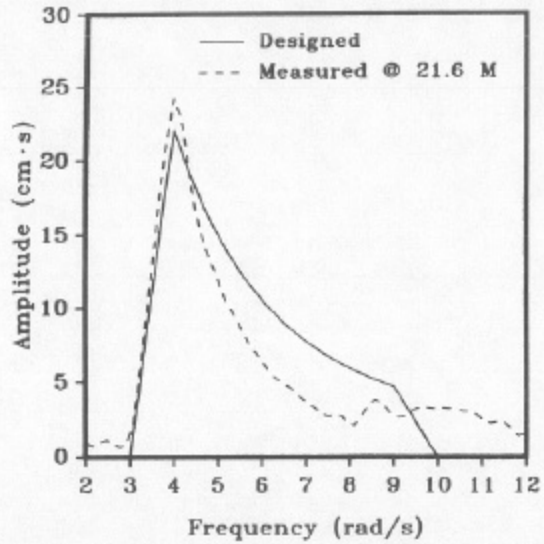

FIG. 1(a). Fourier Amplitude Spectrum of 25-cm Transient Wave

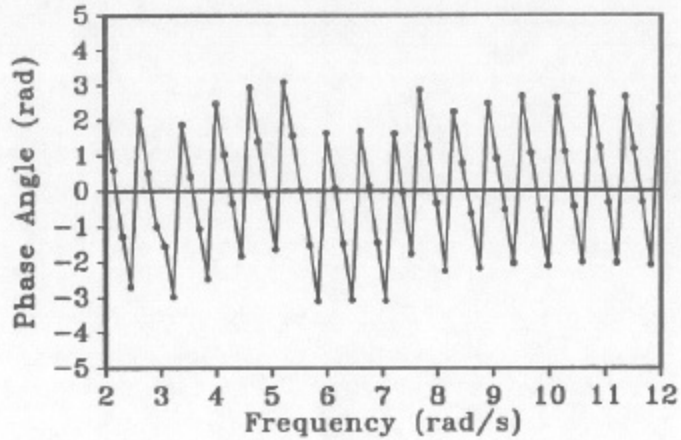

FIG. 1(b). Phase of 25-cm Transient Wave Measured at 21.6 m

asymmetries not present in the Stokes wave, the transient wave kinematics are shown to be much more severe in the crest region above the SWL and somewhat decreased in the region below. This comparison suggests that it would be worthwhile to further investigate the employment of extreme transient waves as more realistic design waves and to develop wave theories that more accurately predict the kinematics in the crest region.

Transient Wave Generation

A transient water wave (TWW) can be thought of as a combination of a finite number of linear waves and represented in the frequency domain as a Fourier spectrum. In the laboratory, a sequence of relatively small component waves is generated such that they meet almost simultaneously, and focus their energy at a given time and downstream location. Since linear waves are primarily characterized by their phase and amplitude, successful creation of a well-focused TWW depends largely on the control of these characteristics. In the synthesis procedure, the variation in amplitude, frequency, phase, and the number of component waves in the resulting time series depends on the design of the Fourier amplitude and phase spectra [Figs. 1(*a*) and (*b*)] for the concentrated TWW, distance from wave maker to test site, and length of the time series.

The size and type of wave-making facilities also impose physical limits on the component waves that can be utilized; consequently there is a limit on the size of the resulting focused TWW. Whether or not that limit is achieved depends on the degree of control exerted on the driving voltage signal, i.e., how well the wave-maker transfer functions are described, order of wave generation used, and the appropriate use of complex corrective transfer functions to account for component wave nonlinearities. The methodology used to generate the transient waves is described in detail by Krafft and Kim (1987) and Kim et al. (1990). This methodology follows that of Takezawa and Hirayama (1977), which emulates ideas presented by Davis and Zarnick (1964), but is further developed with respect to phase and amplitude control of the component waves. Takezawa's controlled synthesis provides for more complete concentration over a relatively shorter duration than previous methods, hence reducing the effects of reflection during model tests. These attributes were considered desirable given the relatively short length (37 m) of the experimental facility in which these tests were conducted.

Using the 25-cm transient water wave as an example, Fig. 2 shows the elevation time series of the resulting focused wave train at the downstream location of maximum concentration of 21.6 m. This particular wave train was designed for maximum concentration at a distance of 20.5 m and time of 50 s. Due to component wave nonlinearities causing small increases in phase speed, the maximum focusing point shifted downstream slightly, with a focusing time of 49.70 s. The transient wave shown in Fig. 2 was reproduced to prototype scale (1:100) in Fig. 3 (bottom) to illustrate the similarity with a wave selected from hurricane Camille time-series data (top). These waves are characterized by their strong asymmetries with respect to both the vertical and horizontal axes. Unlike regular waves, the time series in Fig. 3 clearly shows a greater steepness in the crest front than in the crest rear, a deeper following trough, and vertical asymmetry of the troughs themselves.

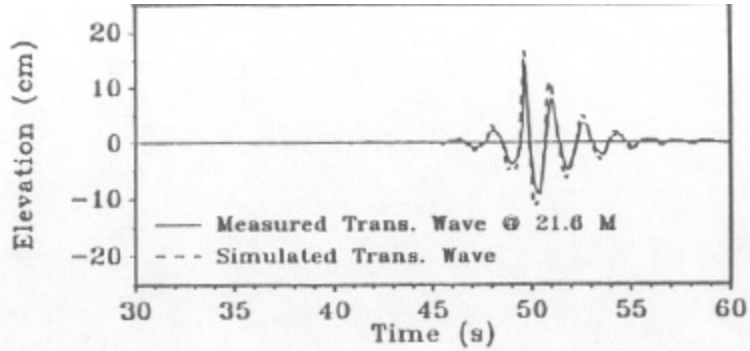

FIG. 2. Measured and Simulated 25-cm Extreme Transient-Wave Elevation Time Series at 21.6 m

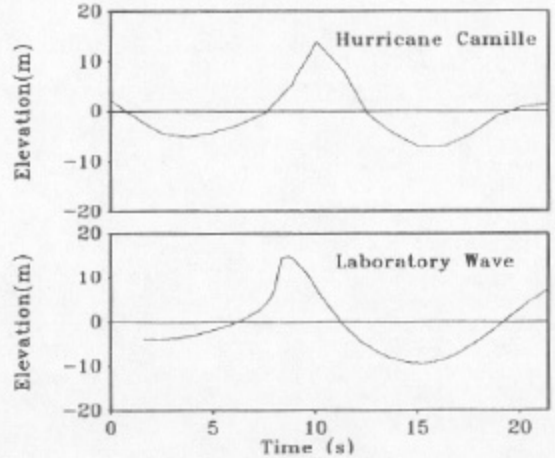

FIG. 3. Time Series of Hurricane Camille and Scaled (1:100) 25-cm Transient Wave

Test Facilities

The experimental measurements were conducted in the wave tank located in the hydromechanics laboratory in the Civil Engineering Laboratory Building at Texas A&M University. The wave tank is 37 m long, 0.91 m wide, and 1.22 m deep and is equipped with a Commercial Hydraulics RSW 90-85 dry back, hinged-flap wave maker, and downstream wave energy-absorbing beach.

A laser Doppler anemometer system was employed for measuring the water particle velocities. This two-dimensional, three-beam laser system, as shown schematically in Fig. 4, consists of an INNOVA four-watt argon-ion laser and DANTEC optics, traverse mechanism, and a frequency tracker and shifter for each velocity component. Real-time signal monitoring of the two velocity components is provided by the data acquisition system (PC-1), employing an IBM PC-XT equipped with an analog to digital (A/D) con-

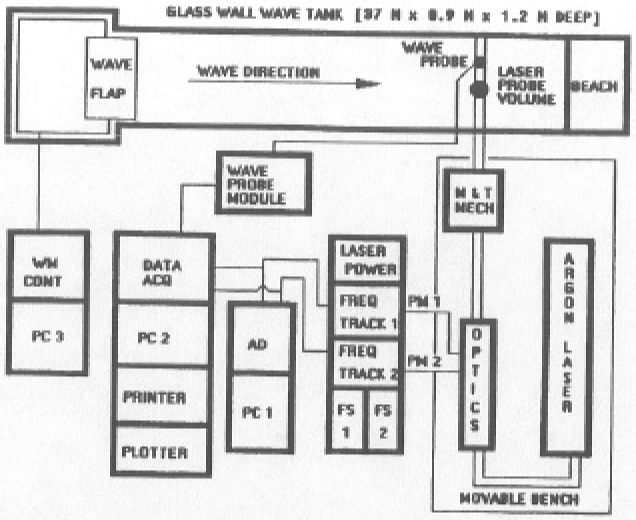

FIG. 4. Schematic of LDA System and Wave-Making Facilities (PC-Computer, FS-Frequency Shifter, PM-Photomultiplier, AD-Analog to Digital Interface, WM-Wave Maker)

verter board and measurement and processing software. The principal data collection and processing system (DATA ACQ) consists of a Hewlett Packard HP-3852A data acquisition system and HP330 controller (PC-2). Software was developed by Boo et al. (1990) for this system to acquire and process LDA velocity data simultaneously with wave elevation data measured by resistance-type wave gauges. The third control system (PC-3) is an IBM PC configured for transmission of the wave-maker driving voltage signal.

The present experiments were performed with the wave flap hinged at a depth equal to the water depth of 0.91 m. The water was seeded with titanium oxide particles, about 0.8 microns in diameter, to ensure the presence of a sufficient amount of suspended solid material to scatter the laser light and result in good velocity signals.

Resistance-type wave gauges were used to measure water surface elevations in the vicinity of the focusing point where the kinematic measurements were made (Fig. 4). The gauges were mounted on an adjustable vernier mechanism that facilitated calibration before each set of experiments. The accuracy of the wave gauges is +/− 0.1 cm. A model length scale of 1:100 was utilized in the synthesis of the waves tested.

Kinematic Measurement Procedures

The LDA was used in the backscatter mode with a 600-mm focal length lens and a mirror and traverse mechanism to precisely position the probe volume 0.3 m away from the side-wall boundary and vertically between the water surface and tank bottom. The Doppler frequency (f) of the backscattered light is directly related to the water particle velocity (u) by:

$$u = \frac{f\lambda}{2 \sin \theta} \qquad (1)$$

where λ = wavelength of the laser beam; and θ = the half-angle of the intersection of the beams. Prior to the start of measurements, the LDA optics were aligned and a zero velocity value was tested by focusing the beam intersection (probe volume) at a fixed point on the tank wall. Frequency tracking range settings were set at either 10–100 kHz or 33–333 kHz. The frequency shift was selected to optimize the range of velocities expected and to facilitate measurement of the oscillating flow. A −50 kHz frequency shift was selected for the 10–100 kHz frequency tracking range and −100 and −200 kHz for the 33–333 kHz range. Accuracy of the velocity measurements is +/−0.005 m/s for the 10–100 kHz range and +/−0.02 m/s for the 33–333 kHz range.

Velocity measurements under the transient waves were made one point at a time. As discussed, the transient wave was generated from a set of component waves that combined at a distance 21.6 m from the wave flap or at a time 49.7 s after initial flap movement. A sampling delay of 49 s was set in the data acquisition software, after which the velocity components were automatically recorded in a serial manner. The velocity data were sampled for a period of 1 s at a rate of 50 samples per second (50 Hz). The maximum velocity normally occurred at 49.7 s +/−0.1 s. For each measurement location under the transient wave, the maximum horizontal and vertical velocity component in three ensembles were averaged. The averaged components were then resolved to give the velocity vector at the measuring point. Since the data is recorded serially, then the waves were generated repeatedly to obtain the complete velocity picture.

The repeatability of the extreme wave was determined to be +/−1 cm. Using linear interpolation of the velocity data along the center three vertical columns of Table 1, the +/−1 cm repeatability results in an average

TABLE 1. Measured Velocities under 25-cm Extreme Transient Water Wave

Elevation[a] (cm) (1)	Distance from Flap (m) 21.3 (2)	21.4 (3)	21.5 (4)	21.6 (5)	21.7 (6)	21.8 (7)	21.9 (8)
			(*a*) Horizontal Velocity (m/s)				
14	—	—	—	1.47	—	—	—
10	—	0.94	0.64	0.95	—	—	—
5	0.57	0.62	0.63	0.63	0.66	0.73	—
0	0.47	0.40	0.51	0.52	0.50	0.59	0.60
−10	0.13	0.14	0.30	0.34	0.29	0.43	0.41
−20	0.10	0.11	0.23	0.25	0.22	0.33	0.31
−30	0.10	0.13	0.19	0.19	0.18	0.26	0.23
			(*b*) Vertical Velocity[b] (m/s)				
14	—	—	—	0.15	—	—	—
10	—	−0.30	−0.39	0.05	—	—	—
5	−0.12	−0.42	−0.42	0.07	−0.03	−0.01	—
0	−0.34	−0.36	−0.19	0.08	0.07	0.03	0.11
−10	−0.29	−0.31	−0.29	0.09	0.14	0.01	0.08
−20	−0.25	−0.24	−0.18	0.04	0.09	0.05	0.08
−30	−0.21	−0.20	−0.15	0.02	0.06	0.02	0.08

[a]Negative wave elevation = below SWL.
[b]Negative vertical velocity = downward.

+/−0.01 m/s velocity variation. The accuracy of the LDA equipment is +/−0.005 m/s for the 10–100 kHz range and +/−0.02 m/s for the 33–333 kHz range. These combine for a velocity uncertainty of 0.015 m/s for the 10–100 kHz range and 0.03 m/s in the 33–333 kHz range.

Results of Kinematic Measurements

Six consecutive profiles of the 25-cm transient wave are illustrated in Fig. 5 at times beginning from 49.58 s and ending at 49.78 s from the initiation of the driving voltage signal. These profiles were measured using a line array of six resistance wave gauges spaced 5 cm apart and parallel to the direction of wave propagation. The crest height of the transient wave is shown to be 15 cm above the SWL at a distance of 21.6 m from the wave flap, which occurred at a time equal to 49.70 s. The last two wave profiles show a second raised portion at 21.9 m due to wave breaking. These profiles clearly indicate the severely asymmetric nature of the wave. The transient wave at 49.70 s has a steeper forward face (asymmetry about vertical axis through crest peak) in the direction of propagation, an elevated crest of nearly 15 cm, a shallow 4-cm leading trough, and a 10-cm following trough (horizontal asymmetries). The difference in crest and trough periods is another significant vertical asymmetry.

Extreme waves with similar shape have been observed in real ocean wave data (Buckley and Stavovy 1981) such as hurricane Camille (Fig. 3). The 25-cm laboratory extreme wave was estimated to have a 1.36 s period and a wavelength of 2.8 m which results in a wave steepness H/L of 0.09 or a wave steepness (ka) of 0.28. If the Camille prototype wave is scaled down using Froude scaling and a 1:100 length scale, then its wave length is 2.1 m and its steepness H/L is 0.1 (1/10) and ka is 0.31. Although not exactly

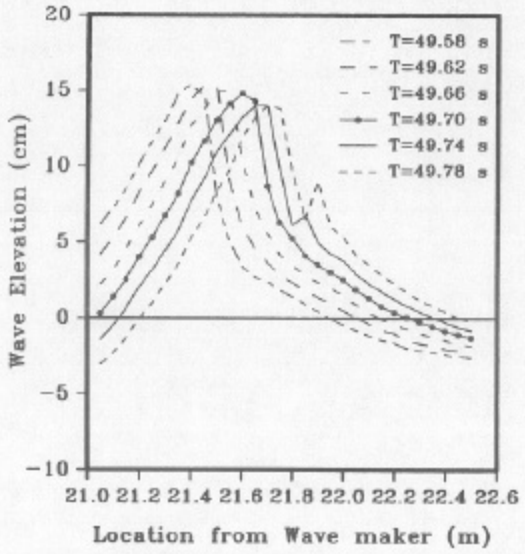

FIG. 5. Measured 25-cm Transient Wave Profiles in Vicinity of Focusing Point of 21.6 m

dynamically similar, i.e., ka of model wave equals ka of prototype wave, the two waves are reasonably close to being dynamically similar.

The horizontal and vertical velocity along seven vertical lines spaced 0.1 m apart in the direction of propagation and at depths relative to the SWL of 14, 10, 5, 0, −10, −20, and −30 cm were measured in the 25-cm wave. These measurements are tabulated in Table 1, and presented graphically as a velocity vector plot in Fig. 6. The results indicate a maximum horizontal velocity of 1.47 m/s measured 1 cm below the crest peak. Along a vertical line directly below the crest peak, the horizontal velocity decreased from 1.47 m/s to 0.52 m/s at the SWL and to 0.19 m/s at −30 cm. The time series of horizontal velocities (Kim et al. 1990) measured under the peak show the maximum velocities occur very nearly directly under the crest peak at all depth elevations. Horizontal velocities in the upstream portion of the wave varied from 0.94 m/s to 0.10 m/s and in the downstream portion from 0.73 m/s to 0.18 m/s.

The vertical velocity did not monotonically decrease with depth below the SWL. A vertical velocity of 0.15 m/s was measured at 14 cm, which decreased to 0.05 m/s at 10 cm, then increased to 0.07 m/s at 5 cm and to 0.09 m/s at −10 cm and then decreased to 0.02 m/s at −30 cm. Vertical velocities in the upstream region of the wave varied from −0.42 to −0.12 m/s with the velocity vectors oriented in the direction of the wave propagation and down. Above the SWL and in the downstream portion of the wave, the vertical velocity was also negative, which resulted in slightly downward directed velocity vectors as shown in Fig. 6, and below the SWL, the velocity vector was slightly upward and in the direction of propagation. Time series data shown by Kim et al. (1990) indicate the vertical velocities directly under the crest peak at all depths was nearly zero. Kinematic behavior qualitatively similar to this has been observed by Skejelbreia (1987).

The measured velocity data under the 25-cm wave were used to numer-

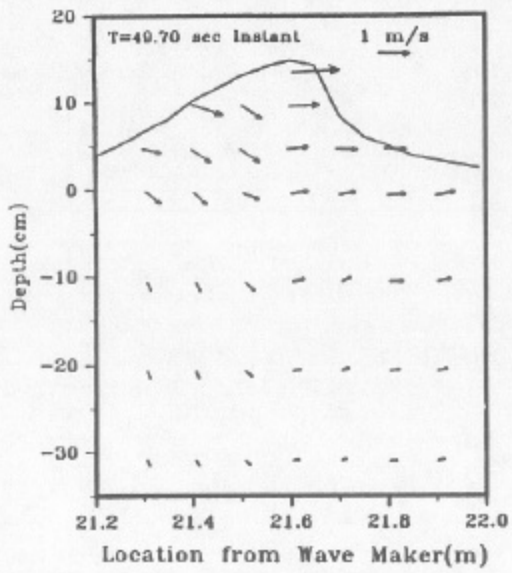

FIG. 6. Velocity Field Under Crest of 25-cm Extreme Transient Wave

ically evaluate the particle acceleration under the wave crest. The relationship between acceleration and velocity is

$$a = \frac{d\mathbf{V}}{dt} \quad \ldots\ldots (2)$$

and the component form is

$$a_x = \frac{\partial u}{\partial t} + u\frac{\partial u}{\partial x} + v\frac{\partial u}{\partial y} \quad \ldots\ldots (3)$$

and

$$a_y = \frac{\partial v}{\partial t} + u\frac{\partial v}{\partial x} + v\frac{\partial v}{\partial y} \quad \ldots\ldots (4)$$

Eqs. (3) and (4) were numerically evaluated using finite difference techniques and the measured velocity data (Table 1). Specifically, a forward difference technique was used to evaluate the time derivative, and the space derivatives were evaluated using a central difference technique with linear interpolation. The acceleration results are tabulated in Table 2 and a vector plot is shown in Fig. 7. Horizontal accelerations in the upstream portion of the wave varied from -3.59 to -0.85 m/s^2 and in the downstream portion from 1.96 to 0.43 m/s^2. Directly under the peak, horizontal accelerations varied from 3.91 m/s^2 at 10 cm above SWL to 0.4 m/s^2 at a point 30 cm below SWL. The vertical accelerations varied between -2.50 and -0.10 m/s^2 in the upstream region of wave and between -4.04 and -0.77 m/s^2 in the downstream region. Directly under the crest, values of -4.73–-0.80 m/s^2 were obtained. The vertical accelerations did not monotonically decrease with depth because of the behavior of the velocity data. The vector plot (Fig. 7) shows the acceleration is directed downward and upstream in the rear of the wave, and it is directed downward and downstream in forward portion and directly under the crest.

TABLE 2. Numerically Determined Acceleration from Measured Velocities under Laboratory-Generated 25-cm Transient Wave

Elevation[a] (cm) (1)	Distance from Flap (m) 21.3 (2)	21.4 (3)	21.5 (4)	21.6 (5)	21.7 (6)	21.8 (7)	21.9 (8)
			(*a*) Horizontal Acceleration[b] (m/s^2)				
+10	—	−3.54	−3.59	3.91	—	—	—
5	−3.40	−2.62	−2.35	2.11	1.96	1.60	—
0	−3.19	−2.18	−2.63	1.84	1.18	0.96	0.99
−10	−2.20	−2.22	−1.33	0.76	0.75	0.85	0.92
−20	−1.46	−1.97	−1.20	0.41	0.72	0.63	0.61
−30	−1.12	−1.35	−0.85	0.40	0.43	0.46	0.50
			(*b*) Vertical Acceleration[c] (m/s^2)				
+10	—	−2.50	−0.52	−3.88	—	—	—
5	−0.72	−1.07	−0.88	−4.73	−4.04	−3.84	—
0	−0.59	−0.26	−0.68	−2.79	−2.82	−2.45	−1.60
−10	−0.33	−0.10	−0.43	−1.63	−1.60	−1.88	−1.43
−20	−0.20	−0.27	−0.81	−0.95	−1.40	−1.48	−1.33
−30	−0.21	−0.30	−0.79	−0.80	−0.88	−0.91	−0.77

[a]Negative wave elevation is below SWL.
[b]Negative horizontal acceleration is in opposite direction of wave propagation.
[c]Negative vertical acceleration is downward.

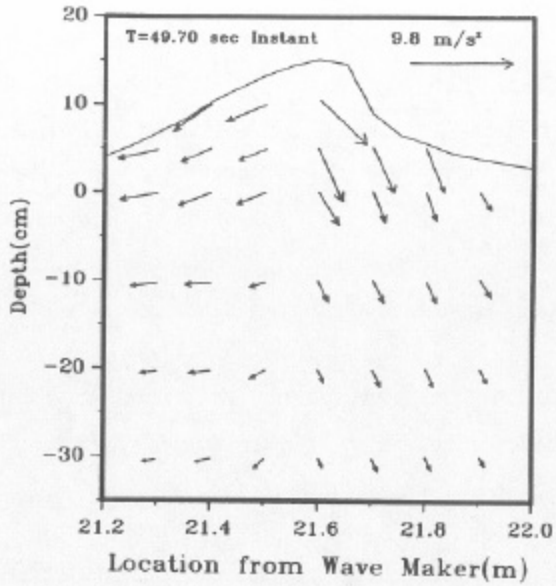

FIG. 7. Acceleration Field Under Crest of 25-cm Extreme Transient Wave

Additional velocity measurements are needed to better evaluate the acceleration near the tip of the crest. The acceleration uncertainty was determined to be approximately 10%, which was based upon the uncertainty of the velocity data. More velocity measurements spaced closer together are expected to reduce the acceleration uncertainty. The 10-cm horizontal and 5–10-cm vertical spacing could be reduced and not approach the repeatability value of $+/-1$ cm. However, the increased number of data points significantly increases the tedious data collection and analysis effort.

Comparison of a Transient and Similar Height Regular Wave

A comparison of similar-height regular wave kinematics to extreme, transient wave kinematics shows the effects of the additional asymmetries found in certain transient waves. A regular wave closely approximated by Stokes third-order wave theory was generated with a wave height of 25 cm and period (1.36 s) similar to the zero upcrossing period of the laboratory transient wave. A time series comparison of the transient, measured regular, and theoretical Stokes wave is illustrated in Fig. 8. The phase velocity of the theoretical Stokes wave was computed as 2.18 m/s. For the transient wave, it was found to be 2.29 m/s, which was computed from six wave elevation time series recorded at 5-cm intervals in the vicinity of maximum concentration. As shown in Fig. 8, the wave heights for the transient and regular wave are essentially the same, but the theoretical Stokes wave has

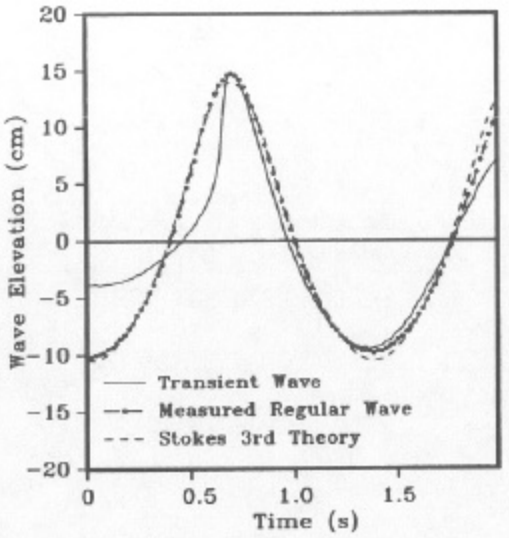

FIG. 8. Elevation Time Series for Laboratory Transient, Regular, and Theoretical Stokes Waves

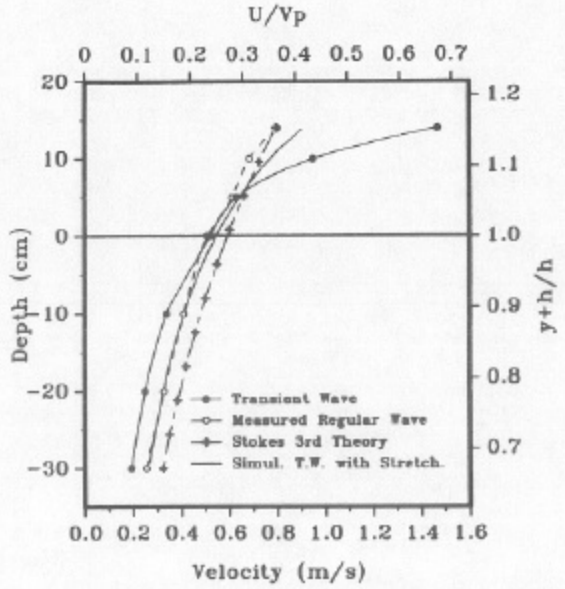

FIG. 9. Comparison of Measured Horizontal Velocity under Crest Peak of 25-cm Transient Wave, Similar Height Regular Wave, Stokes Third-Order Theory, and Simulated Transient Wave with Stretching

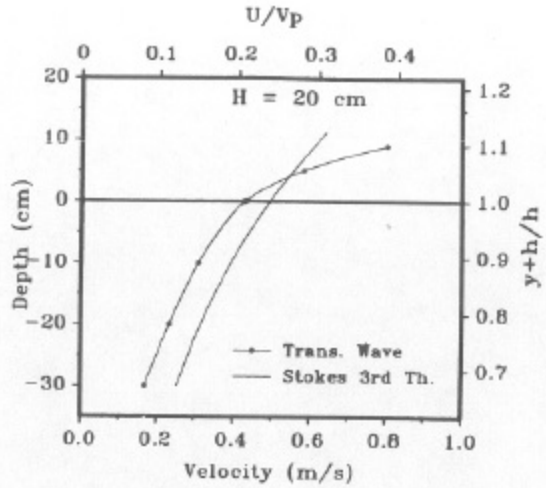

FIG. 10. Comparison of Horizontal Velocity under Crest of Transient Water Wave of 20-cm Wave Height with Stokes Third-Order Theory

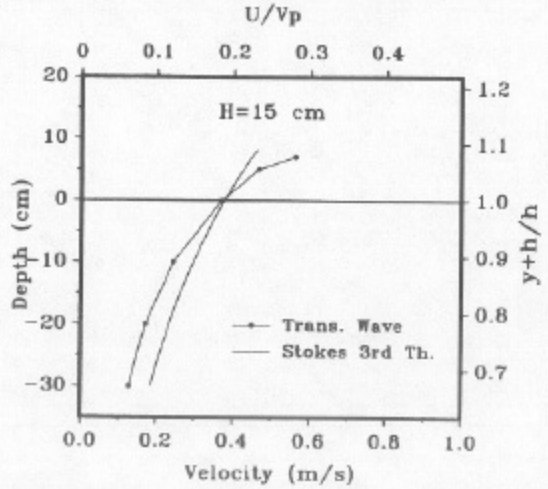

FIG. 11. Comparison of Horizontal Velocity under Crest of Transient Water Wave of 15-cm Wave Height with Stokes Third-Order Theory

a slightly lower crest and deeper trough. The transient wave has a noticeably different trough level preceding and following the wave crest, which is typical for large, laboratory generated transient waves and for some of the extreme waves recorded during severe storms.

Velocity measurements were made at the same depths under the regular wave as were made for the transient wave, and the results are illustrated in Fig. 9. At a 14-cm elevation the horizontal velocity under the regular wave was measured as 0.80 m/s. This value is 54% of the value measured at the same location under the transient wave. The measured regular wave values at 10-, 5-, 0-, −10-, −20-, and −30-cm elevations were 72%, 98%, 98%,

TABLE 3. Horizontal Velocity of Transient Wave According to Wave-Height Variations

Depth (cm) (1)	Wave Height (cm) 25 (2)	22 (3)	20 (4)	18 (5)	15 (6)
14	1.47	—	—	—	—
12	—	1.00	—	—	—
10	0.95	0.88	—	—	—
9	—	—	0.80	—	—
8	—	—	—	0.67	—
7	—	—	—	—	0.56
5	0.63	0.60	0.58	0.53	0.47
0	0.51	0.48	0.43	0.41	0.37
−10	0.34	0.32	0.31	0.28	0.25
−20	0.25	0.24	0.23	0.20	0.17
−30	0.19	0.18	0.17	0.15	0.13

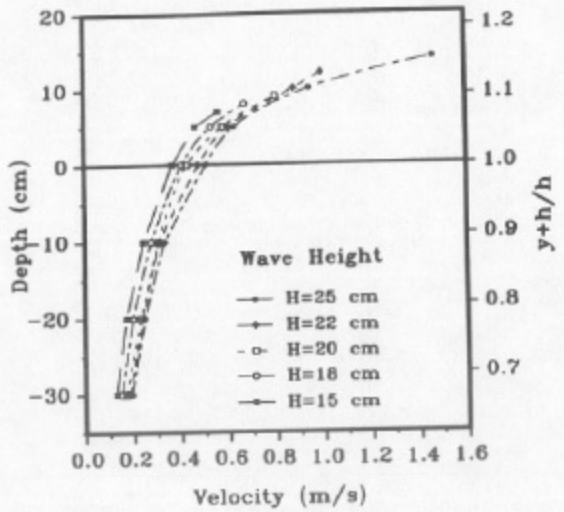

FIG. 12. Effect of Wave Height on Maximum Horizontal Velocity under Transient Waves

121%, 132%, and 135% of the velocity values measured in the transient waves at the same elevations, respectively. Fig. 9 indicates that velocities above the SWL were considerably higher in the transient wave, and below the SWL were smaller than those in the regular wave. Theoretical results using Stokes third-order theory in a similar figure by Kim et al. (1990) are in error and the correct values are shown in Fig. 9. This figure shows the Stokes third-order theory overpredicts the velocities below the SWL. The 0.59 m/s theoretical velocity at the SWL is 13% greater than the TWW value of 0.52 m/s. The maximum velocity of Stokes third-order wave at 14 cm above SWL is 54% of the maximum velocity of the transient wave. This represents a significant difference in the kinematics of the transient wave

and the regular Stokes-type wave often used in design calculations, and it points out the need to use such a transient wave for more realistic wave force values.

Comparison of Measured and Simulated Horizontal Velocity under Crest of Transient Wave

A simulation of the horizontal velocity of the 25 cm transient wave is completed using linear wave theory and linear superposition principle.

First, the fast Fourier transform of the measured time history of the 25 cm transient wave (Fig. 2) yields the amplitude and phase [Figs. 1(*a*) and (*b*)]. Superposition of the 30 component waves yields the simulated transient wave elevation

$$\eta(t) = \sum_{i=1}^{N} a_i \cos(k_i x - \omega_i t + \phi_i) \quad \ldots\ldots (5)$$

With the assumption that the measured location x is zero, the horizontal velocity at $(0,y,t)$ is

$$u(0,y,t) = \sum_{i=1}^{N} \omega_i a_i \frac{\cosh k_i(y + h)}{\sinh k_i h} \cos(-\omega_i t + \phi_i) \quad \ldots\ldots (6)$$

where a_i = wave amplitude; k_i = wave number; ω_i = circular frequency; ϕ_i = phase angle; and h = water depth.

The horizontal velocity can be determined by applying Wheeler stretching or Delta stretching procedures. Wheeler's (1970) formula is

$$y_e = (y_a + h)\frac{h}{h + \eta} - h \quad \ldots\ldots (7)$$

where y_e = the effective vertical coordinate ($-h \le y_e \le 0$); y_a = the actual vertical coordinate ($-h \le y_a \le \eta$); and η = the elevation of instantaneous free surface (positive upward and zero at SWL). Using (7), the velocity at the effective coordinate is mapped into that at the actual coordinate.

The component waves [Figs. 1(*a*) and (*b*)] are superposed as shown in Fig. 2. It is interesting to note that the simulated elevation is larger than the measured. The simulated wave is symmetric about the vertical axis while the measured is asymmetric. The simulated and stretched velocity is compared with others as shown in Fig. 9. The simulated velocity is very close to that of the symmetric large regular wave in the region below SWL, while it is slightly larger than the regular wave velocity in the region above SWL. The simulated wave is also compared with the measured transient wave velocity. It is larger than that of the transient wave in the region below SWL whereas it is much less than that of the measured transient wave in the region above. The maximum of the simulated velocities is 61.4% of the maximum measured value. This represents a significant difference in the kinematics of the simulated and measured transient wave. It is concluded from the foregoing comparison that use of linear wave theory and linear superposition with Wheeler stretching apparently does not yield a reasonably good simulation. This is attributed to the fact that the laboratory generated energy focused wave has gone through a complicated nonlinear interaction among the component waves during progression.

Figs. 10 and 11 show a comparison of velocities from Stokes third-order

wave theory to the horizontal velocity measured directly under the crest of transient water waves of 20-cm and 15-cm height as a function of water depth. Horizontal velocities, u, are nondimensionalized by phase velocities, V_p, of Stokes third-order wave corresponding to a wave height of 25, 20, and 15 cm, respectively. As shown, the horizontal velocities in the upper two-thirds of the crest of the transient waves are underestimated by Stokes third-order theory, and below that they are overestimated. New theories are needed to more closely predict the velocities in and below the crest.

Effect of Transient-Wave Height on Crest Velocity

Transient waves of 25-, 22-, 20-, 18-, and 15-cm wave height were generated, and the vertical and horizontal velocities were measured directly under the crest at several elevations. The measured horizontal crest velocities at various elevations under the crest are tabulated in Table 3. The vertical velocities were near zero as expected under the crest. The effect of the variation of height on the crest horizontal velocity is illustrated in Fig. 12. The results show that the horizontal velocity decreases as the height decreases at all elevation levels. The maximum horizontal velocity near the crest (within 2 cm) decreased from 1.47 m/s, 1.0 m/s, 0.81 m/s, 0.67 m/s, and 0.56 m/s for the 25-, 22-, 20-, 18-, and 15-cm waves, respectively. At the SWL the maximum horizontal velocities decreased from 0.63 m/s for the large wave to 0.46 m/s for the smallest wave. At the lowest elevation (-30 cm) the velocity decreased from only 0.19 to 0.13 m/s. Thus, the reduction in horizontal velocity under the crest diminished with wave height and decreased as the distance from the free surface increased.

Summary and Conclusions

Laser Doppler anemometer measurements of the velocity field were completed beneath the crest of laboratory-generated transient waves varying in height from 25 cm to 15 cm. The largest wave (25 cm) was similar in size and asymmetric properties to that found in a hurricane Camille wave. The effect of wave height on the horizontal velocities shows the maximum horizontal velocities decrease as the wave height decreases.

For the large 25-cm transient wave, the maximum measured velocity was 1.47 m/s at 14 cm above the SWL and directly under the crest peak just prior to breaking. This value is 64% of the measured phase velocity of the transient wave and 184% of the velocity measured at the same elevation under a similar height regular wave. Comparison of measurements of the equivalent regular wave with the large transient wave showed the horizontal velocities in the 25-cm transient wave were larger in the region above SWL to the crest peak. Below the SWL and under the crest peak the velocities in the transient wave were smaller than those measured in the regular wave. Thus, the kinematics of an extreme transient wave are considerably different from a regular wave of the same height and period.

The capability of measuring velocities during the very short time interval when the tip of the wave crest enters and exits the probe volume was demonstrated. For the particular transient waves tested, measurements were obtained to within 1 or 2 cm of the water surface at the crest peak.

The velocity data collected under the large transient wave along several vertical transects through the wave were used to numerically evaluate the acceleration in the crest region. The maximum horizontal and vertical accelerations were 3.9 and -4.7 m/s^2, which were located 4 and 9 cm below the peak of the wave, respectively.

The stretching method used in this research for predicting the horizontal velocity of the simulated and transient wave greatly underestimated the measured horizontal velocity at the free surface for the transient wave. Below the still-water level the stretching technique overestimates the maximum horizontal velocity. Thus, the superposition method with stretching is not adequate for evaluating the kinematics of an extreme transient wave.

The study results indicate that both the design wave and random wave approaches may underestimate the loads on structures caused by a steep extreme wave. Therefore, new theoretical and/or empirical techniques need to be developed to predict the kinematics under transient waves.

It is both important to reproduce and analyze extreme, nonlinear wave forms in the laboratory, but further research is needed to identify which observed wave forms occurring in nature should be modeled. Based on the present findings and those of several recent investigations, a better method of design for extreme transient waves is needed for estimating maximum loads on offshore structures, which includes the effects of extreme wave asymmetries.

Acknowledgment

The research reported in this paper was conducted for the Offshore Technology Research Center, which is supported in part by the National Science Foundation Engineering Research Centers Program grant #CDR-8721512.

Appendix I. References

Birkinshaw, M., Easson, W. J., Greated, C. A., and Webb, R. M. (1988). "Breaking wave design: A case history." *Proc. Inst. Civ. Engrs.*, Part 2, 85, 415–433.

Boo, S. Y., Kim, C. H., and Randall, R. E. (1990). "Software development for the measurement of wave kinematics and procedures for using laser doppler anemometer." *Offshore Technology Research Center Final Report*, Texas A&M Univ., College Station, Tex.

Buckley, W. H. (1983). "A study of extreme waves and their effects on ship structure." *The Ship Structure Committee Report No. SSC-320*, The Ship Structure Committee.

Buckley, W. H., and Stavovy, A. B. (1981). "Progress in the development of structural load criteria for extreme waves." *Proc. Extreme Loads Response Symp.*, The Ship Structure Committee and the Society of Naval Architects and Marine Engineers.

Davis, M. C., and Zarnick, E. E. (1964). "Testing ship models in transient waves." *Proc. 5th Symp. on Naval Hydrodynamics*, Bergen, Norway.

Dean, R. G., and Dalrymple, R. A. (1984). *Water wave mechanics for engineers and scientists*. Prentice Hall Inc., Englewood Cliffs, N.J.

Dommermuth, D. G., Yue, D. K. P., Lin, W. M., Rapp, R. J., Chan, E. S., and Melville, W. K. (1988). "Deepwater plunging breakers: A comparison between potential theory and experiments." *J. Fluid Mech.*, 189, 423–442.

Forristall, G. Z. (1981). "Kinematics of directionally spread waves." *Proc. ASCE Conference on Directional Wave Spectra Applications*, ASCE, Sept., 129–166.

Gudmestad, O. T. (1990). "A new approach for estimating irregular deep water wave kinematics." *J. Appl. Oc. Res.*, 12(1), 76–88.

Gudmested, O. T., and Connor, J. J. (1986). "Engineering approximations to nonlinear deepwater waves." *J. Appl. Oc. Res.*, 8(2), 76–88.

Kim, C. H., Randall, R. E., Krafft, M. J., and Boo, S. Y. (1990). "Experimental

study of kinematics of large transient wave in 2-D wave tank." *Proc. of the 22nd Annual Offshore Tech. Conference*, May, Houston, Tex.
Kjeldsen, S. P. (1989). "The experimental verification of numerical models of plunging breakers." *Proc. Coastal Engrg. Conference*, 15–30.
Kjeldsen, S. P., Vinje, T., Myrhaug, D., and Brevig, P. (1980). "Kinematics of deep water breaking waves." *Proc. 12th Annual Offshore Tech. Conference*, Houston, Tex.
Krafft, M. J., and Kim, C. H. (1987). "Extreme transient water wave generation at Texas A&M University." *COE Report 294*, Civil Engrg. Dept., Oc. Engrg. Program, Texas A&M Univ.
Longuet-Higgins, M. S. (1974). "Breaking waves in deep and shallow water." *Proc. 10th Symp. on Naval Hydrodynamics*, Massachusetts Institute of Technology.
Mansard, E. P. D., and Funke, E. R. (1982). "A new approach to transient wave generation." *Proc. 18th Int. Conference on Coastal Engrg.*, Cape Town, South Africa.
Rapp, R. J. (1986). "Laboratory measurements of deep water breaking waves," dissertation, presented to Massachusetts Institute of Technology, at Cambridge, Massachusetts, in partial fulfillment of the requirements for the degree of Doctor of Philosophy.
Rodenbusch, G., and Forristall, G. Z. (1986). "An empirical model for random directional wave kinematics near the free surface." *Proc. 18th Annual Offshore Tech. Conference*. May, Houston, Tex.
Skjelbreia, J. E. (1987). "Observation of breaking waves on sloping bottoms by use of laser Doppler velocimetry." *Report No. KH-R-48*, California Inst. of Tech. Pasadena, Calif.
Takezawa, S., and Hirayama, T. (1977). "Advanced experimental techniques for testing ship models in transient water waves: Part II, the controlled transient water waves for using in ship motion tests." *IMechE*, 37–54.
Vugts, J. H., and Bosma, J. (1981). "Wave kinematics and fluid loading in irregular waves." *Int. Symp. on Hydrodynamics in Oc. Engrg.*, Aug., Trondheim, Norway.
Ward, E. G. (1979). "Ocean data gathering program—An overview." *Proc. 6th Annual Offshore Tech. Conference*, May, Houston, Tex.
Wheeler, J. D. (1970). "Method for calculating forces produced by irregular waves." *J. Petroleum Tech.*, Mar., 359–367.

Appendix II. Notation

The following symbols are used in this paper:

a = wave amplitude or acceleration;
a_x = horizontal acceleration;
a_y = vertical acceleration;
d = total derivative;
f = Doppler frequency;
g = gravitational acceleration;
H = wave height;
h = water depth;
k = wave number;
L = wave length of water wave;
t = time;
u = horizontal water particle velocity;
$\mathbf{V}$ = velocity vector;
V_p = phase velocity;
v = vertical water particle velocity;
x, y = horizontal and vertical coordinate axes;
y_a = actual vertical coordinate;

y_e = effective vertical coordinate;
ϕ = phase angle;
θ = half angle of intersection of laser beams;
λ = wavelength of laser beam; and
η = wave elevation.